

Optical and Structural Properties of Tin Sulfide Nanoparticles Obtained via Solvothermal Routes

Jerry O. Adeyemi,^[a,b] Opeyemi A. Oyewo,^[c] and Damian C. Onwudiwe^{*[a,b]}

Abstract. The effect of using different solvothermal approaches, involving heat-up and hot-injection routes, on the phase, morphology and optical properties of tin sulfide nanoparticles using novel dibutyltin(IV) *p*-methylphenyl dithiocarbamate as single source precursor compound have been studied. Dibutyltin(IV) *p*-methylphenyldithiocarbamate was synthesized and characterized using various spectroscopic techniques (FT-IR, ¹H, ¹³C and ¹¹⁹Sn), and elemental analysis. TG analysis, studied under nitrogen, revealed tin sulfide of the rare mixed-valence binary phase (Sn₂S₃) as the final residue at the end of the decomposition process. The samples presented as SnS1 and SnS2

obtained by the heat-up and hot injection routes respectively, at 220 °C and in the presence of oleylamine as surfactant, revealed the α -cubic phase of SnS with Herzenbergite structure. The X-ray diffraction analysis of the nanoparticles also revealed patterns which showed preferred growth along (111) orientation; hence, favoring anisotropic shapes which were more distinct at higher magnification images of the TEM as a pseudo spherical morphology tending toward the formation of short rods. The optical property of the nanoparticles exhibited a blue shift in the bandgap energy with respect to the bulk, which is an evidence of quantum confinement effect.

Introduction

Semiconductors with narrow bandgaps and near-infrared optical activity have been of interest lately.^[1] In these group, tin sulfide has received considerable attention because of its natural abundance, low cost, and environmental friendliness.^[1] Tin sulfide exists in various forms; hence, possesses different bandgap energies of 1.3 eV (SnS), 2.18 eV (SnS₂), and 0.95 eV (Sn₂S₃). Due to the low toxicity of these materials, they have been applied as solar energy absorber in holographic recording and for infrared detection. The tin sulfide (SnS) phase, possesses desirable properties such as high absorption properties and high hole mobility, which favors its incorporation in solar cells materials for photovoltaic application.^[2] Its electronic bandgap, which lies between that of Ga and Si, has attracted much attention.^[3] Furthermore, SnS has both indirect and a direct bandgap (1.09 and 1.3 eV, respectively) in the spectral region required of materials used as efficient collectors of solar radiation. It has high optical absorption coefficient for photons with energies greater than 1.3 eV.^[4]

Studies have shown that the nature of tin content in SnS nanoparticles may influence its conducting properties and determines if the SnS will be a n-type or p-type conductor.^[3]

Tin(II) sulfide (SnS) has a distorted rock salt structure which is isostructural with germanium sulfide, in which six sulfur atoms surround each tin atom, which has three short Sn–S bonds within the layer and three long bonds attached to the sulfur atoms in the next layer.^[5] These layers in SnS are joined with weak van der Waals forces; thus, providing an intrinsic chemically inert surface without dangling bonds and surface density.^[6] This is responsible for the surface of the SnS being devoid of Fermi level pinning.^[6]

Different methods have been employed for the synthesis of tin sulfide nanomaterials. The synthetic routes influences their properties and determines their applications.^[7] The synthesis of tin sulfide nanoparticles via the solvothermal decomposition of single source precursor compounds is not widely reported in literature compared to other routes such as wet chemical route,^[8] modified solution dispersion method,^[9] and physical deposition methods^[10]. *Kergommeaux* et al. have synthesized tin sulfide nanoplatelets using the colloidal method of synthesis, which involved Tin(IV) chloride pentahydrate, and thioacetamide as the tin and sulfur precursors respectively in oleylamine.^[11] Furthermore, tin sulfide obtained via a modified solution dispersion involving the direct dispersion of melted tin in a sulfur-dissolved solvent has been reported.^[9]

Solvothermal method via single source decomposition involves the decomposition of a single source precursor in high boiling point solvents at a temperature beyond the stability of the compound.^[12] These high boiling point solvents possess coordinating groups such as thiols or amines, and act as capping agents.

Dithiocarbamate ligands have shown exceptional binding ability with most metals (transition metals, main group metals, and lanthanides) to form complexes.^[13,14] These complexes have been widely applied in agriculture, industries, and medicine.^[13] They have also proven as useful single source precursor for the synthesis of metal sulfide nanoparticles because of

* Prof. D. C. Onwudiwe
E-Mail: Damian.Onwudiwe@nwu.ac.za

[a] Department of Chemistry
Faculty of Natural and Agricultural Science
North-West University (Mafikeng Campus)
Private Bag X2046
Mmabatho 2735, South Africa

[b] Material Science Innovation and Modelling (MaSIM) Research
Focus Area
Faculty of Natural and Agricultural Science
North-West University (Mafikeng Campus)
Private Bag X2046
Mmabatho, South-Africa

[c] Department of Chemical, Metallurgical and Materials Engineering
Tshwane University of Technology
Pretoria, 0001, South Africa

the direct metal to sulfur bond in their structure.^[14,15] Different derivatives of dithiocarbamate ligands can influence the properties of the nanoparticles such as size and shape.^[16,17] A number of organotin(IV) dithiocarbamate complexes have been used to prepare different phases of tin sulfide nanoparticles via thermal process.^[15,18–20] However, only few reports involved their use as single source precursors in the presence of coordinating solvent.

In this study, a novel complex of dibutyltin(IV) *p*-methylphenyldithiocarbamate was employed as single source precursor to tin sulfide nanoparticles using two methods of solvo-thermal synthesis: the heat-up and hot-injection routes. The complex was well characterized, and the optical and structural properties of the synthesized nanoparticles were studied using XRD, TEM, and absorption spectroscopy.

Results and Discussion

Synthesis of the Complex

The complex preparation followed an already established method of synthesis involving the reaction of dithiocarbamate ligand, NaL, and dibutyltin(IV) in a 2 to 1 stoichiometric mole ratio.^[21] The reaction proceeded by the substitution of all the available chloride ions present in the organotin(IV) chloride. The complex was easily purified by recrystallization and the product obtained as white precipitate, which was sparingly soluble in alcohols and completely soluble in dimethylsulfoxide, dichloromethane and chloroform. This complex was solvo-thermally decomposed (using the heat-up and hot injection routes), to afford dark grey precipitates which were soluble in toluene.

Spectroscopic Studies

Useful information was deduced from the selected FT-IR peaks due to the wide studies on dithiocarbamate and its complexes. The complex showed bands around 1516 cm^{-1} , which was attributed to the partial double bond character of C–N stretching vibration. A strong band at 1004 cm^{-1} , ascribed to C–S stretching vibration, suggested a bidentate coordination between the tin and the dithiocarbamate ligand.^[22] A band observed at 546 cm^{-1} was ascribed to the Sn–C bond and, thus, supports the presence of the organotin(IV) moieties.^[23] Furthermore, a low intensity peak at 366 cm^{-1} due to the presence of the Sn–S bond was also observed.^[24,25]

In the ^1H NMR spectrum, the aromatic protons were observed downfield as multiplet in the region 7.47–7.12 ppm. A signal at 2.50 ppm was ascribed to the protons of the methyl group in the para position of the phenyl ring of the ligand moiety. The signal observed at a higher frequency at about 5.29 ppm, was attributed to the proton of the N–H; and the position was due to the electronegative N atom.^[26,27] The signals due to the methyl and methylene protons on the dibutyltin(IV) moiety were found in the range 2.31–0.90 ppm.^[28]

The ^{13}C NMR spectrum showed a weak signal at 192 ppm, due to the carbon of the thioureide ($-\text{NCS}_2$) group. The region of appearance of this peak suggested the contribution of the double bond character of the thioureide group of the dithiocarbamate moiety.^[29] The signals due to the aromatic carbons of the ligand moiety resonated in the range 136–123 ppm,^[26] whereas the signal of the *para*-methyl carbon resonated around 21 ppm.^[29] The carbon signal attributed to the methylene and methyl groups in the organotin(IV) moiety were found in the range 30–13 ppm.

The ^{119}Sn spectrum showed peak at -312 ppm , suggesting a hexacoordinate arrangement around the Sn metal.^[21]

Thermogravimetric Analysis of the Complex

The TG/DTG plot of the complex, showed three decomposition pathways as presented in Figure 1. The data obtained from the thermogravimetric plots have been summarized in Table 1. The first step of decomposition of the complex occurred between 98–162 °C, and this resulted into about 17.65 % loss of the starting mass attributed to $\text{CH}_3-\text{C}_6\text{H}_4$ from the dithiocarbamate group of the complex. After this stage, the complex further decomposed (in a second step) in the range 163–188 °C, releasing about 20 % of the starting mass which was attributed to the butyl group from the organotin moiety and the remaining mass was about 80 % of the starting mass. This agreed with the calculated value (81.17 %) of the found mass at this stage. This step was subsequently followed by a third and final step in a temperature range of 211–303 °C. The mass of the residue found was 53.97 % of the starting mass and this agrees with the calculated value Sn_2S_3 (54.80 %). The phase of tin sulfide residues observed here was similar to what has been reported in literature for organotin(IV) pyrrolidinedithiocarbamate complexes,^[15] and the phase of the residue was dependent on the ligand moiety as well as temperature. Thus, indicating their potential as a single source precursor for tin sulfide nanoparticles.

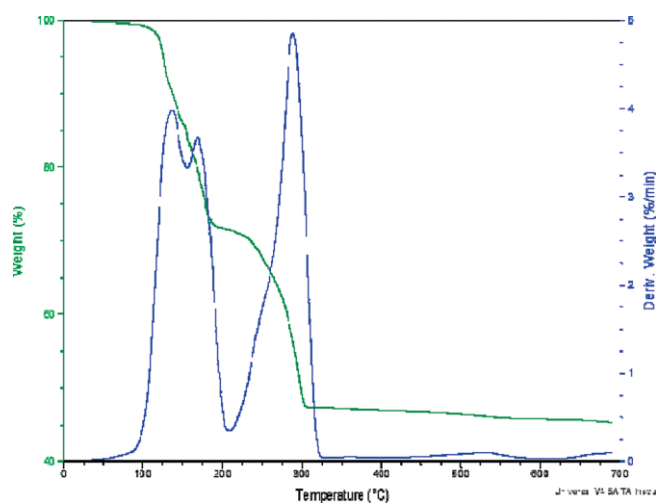


Figure 1. TG/DTG curves obtained in an inert atmosphere at heating rate $10\text{ K}\cdot\text{min}^{-1}$ for complex $[(\text{C}_4\text{H}_9)_2\text{SnL}_2]$.

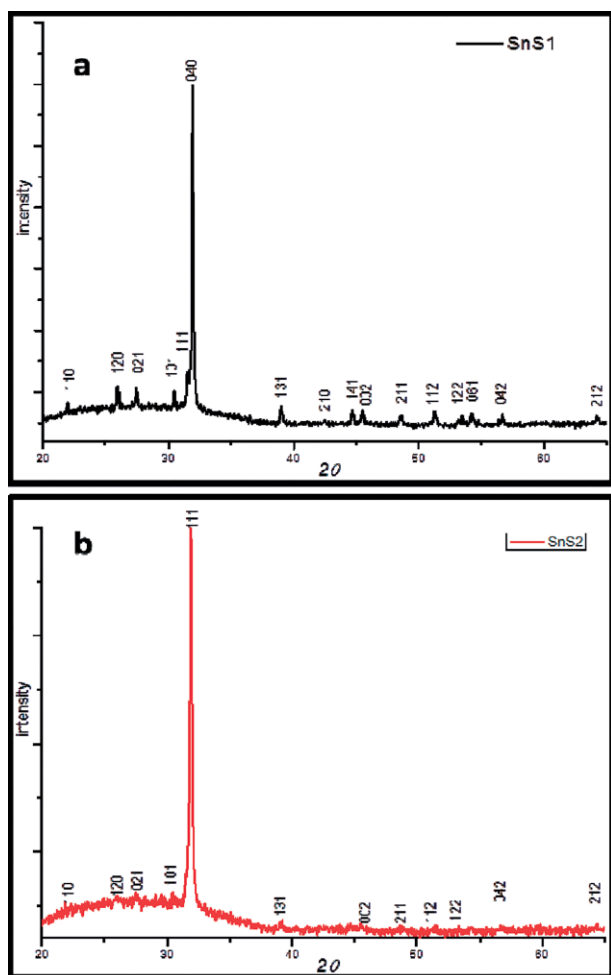


Figure 2. XRD pattern of tin sulfide nanoparticles obtained from $[(C_4H_9)_2SnL_2]$ using (a) heat-up route-SnS1 and (b) hot injection-SnS2.

Table 1. Thermal analysis data of the complex.

	$[(C_4H_9)_2SnL_2]$
Temperature range of decomposition /°C	
1st stage	98–162
2nd stage	163–188
3rd stage	211–303
DTG peak temperature /°C	
1st stage	157
2nd stage	168
3rd stage	294
Product obtained	
1st decomp.	$(CH_3-Ph)H(NCS_2)_2Sn(But)_2$
2nd decomp.	$(CH_3-Ph)H(NCS_2)_2Sn$
3rd decomp.	Sn_2S_3
Mass of residue /mg, found (calcd.)	
1st stage	13.96 (13.96)
2nd stage	13.56 (13.76)
3rd stage	8.98 (9.29)

X-ray Diffraction Study of the Nanoparticles

The X-ray diffraction patterns of the nanoparticles obtained from both method of synthesis is presented in Figure 2. The

diffraction patterns of the particles obtained via the solvothermal routes were similar. The patterns of the nanoparticles from the heat-up route showed peaks indexed as (120), (021), (101), (111), (131), (210), (002), (211), and (061), which corresponded to orthorhombic phase of SnS (JCPDS no. 39–0354).^[30] This phase, which has a herzenbergite structure, possesses a lattice parameter $a = 4.3$, $b = 11.2$, $c = 4.0$ Å, and $Z = 4$. The pattern showed that the $2\theta = 31.53^\circ$ indexed as (111) was the preferred orientation growth of the nanoparticles.^[31] The absence of peaks characteristic of other phases of tin sulfide such as SnS_2 , the oxidized form of tin, i.e. SnO_2 and atomic tin – Sn, indicated the purity of the obtained SnS phase. Using Debye–Scherrer equation, which shows the relationship between the size of the particle, full width at half maximum (FWHM) of the strongest peaks in SnS1 and SnS2 (indexed (111) and (040) respectively) (β) and the wavelength (λ) of the nanoparticles, the average crystalline size (D) of the nanoparticles were obtained. The sizes found were in the range 63–65 nm for both SnS1 and SnS2. The observed orientation of these particles suggested the growth process was controlled by nucleation, which is in agreement with some of the studies reported on SnS nanoparticles.^[32]

Morphology of the Synthesized SnS Nanoparticles

The images obtained from the TEM analysis of the synthesized nanoparticles are presented in Figure 3a and Figure 4a. These images showed slight agglomeration of the particles, whose shape could be described as pseudo-spherical (with a tendency towards the formation of short rod) is presented in Figure 3a and Figure 4a. The particle size distributions are presented as histograms in Figure 3b and Figure 4b for SnS1 and SnS2, respectively. The selected area electron diffraction (SAED) presented as inset in Figure 3a and Figure 4a showed the formation of circular ring, attributed to polycrystalline nature of the SnS nanoparticles.^[8] The estimated average particle size was found in the range of 62–66 nm for SnS1 and SnS2, which is in agreement with the size estimation from the XRD patterns.

The used capping agent, oleylamine, is a long-chain primary alkyl-amine, which has been used widely for nanoparticle synthesis as solvent for organic and inorganic compounds, reducing agent and as surfactant. Studies have shown it to produce rods with low regularity and fewer chances for long range organization which is attributed to its “cis” configuration and buckled molecular chain.^[33] This may suggest the reason for the obtained morphology in both nanoparticles prepared.

Optical Properties

The optical properties of semiconductors are very important for their application in photoconductors, near-infrared detectors, and photovoltaic materials. Quantum-size effect for a semiconducting material can easily be manipulated by fine-tuning the size of the semiconductor.^[34] In semiconductor nanoparticles, an abrupt increase in the absorption wavelength, which matches with the bandgap energy could result due to the optical excitation of electrons across the bandgap. This is

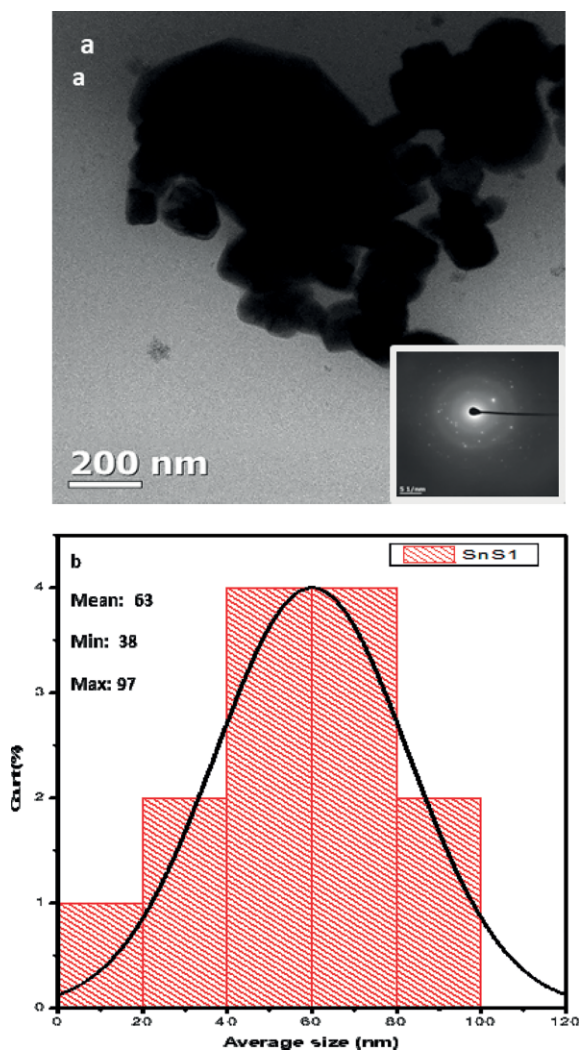


Figure 3. (a) TEM images of SnS1 with the corresponding SAED pattern (inset) and (b) the size distribution histograms.

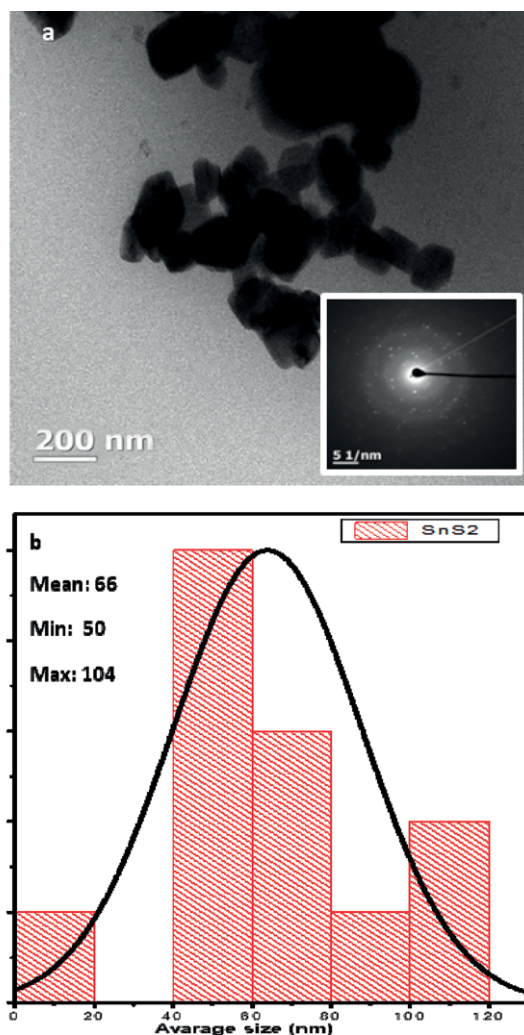


Figure 4. (a) TEM images of SnS2 with the corresponding SAED pattern (inset) and (b) the size distribution histograms.

known as the band edge energy.^[35] The properties such as shape, size, size distribution and types of surfactants used can influence the shape of the absorption shoulder and the band edge position of a nanoparticle. Thus, for semiconductors, the size of the nanoparticles could be estimated from the position of the absorption band edge.^[35] The optical properties of the obtained SnS nanoparticles have been analyzed using absorption spectroscopy. Figure 5a and b shows the absorbance spectra of the nanoparticles with their respective Tauc plots. The spectra show absorption peak around 831 and 875 nm for **SnS1** and **SnS2**, respectively. The bandgap energy (E_g) for these nanoparticles was obtained from the spectral using the near-band edge absorption relation [Equation (1) and Equation (2)]:^[30]

$$(ahv)^n = A(hv - E_g) \quad (1)$$

$$a = \frac{A \rho}{M c l} \quad (2)$$

where $h\nu$ is the photon energy and A is a constant, which has different values based on different transition, n characterizes the transition. When $n = 2$ and $2/3$ the transition is said to be direct allowed transition, and it is an indirect allowed transition when $n = 1/2$ and $= 1/3$. M is the molecular weight, ρ is the density, c is the sample concentration dispersed in toluene, l is the path length of light. Thus, the direct bandgap energies (E_g) of the nanoparticles were obtained by plotting the graph of $(ahv)^2$ against $h\nu$ at the point where $a = 0$,^[36] as presented in Figure 5b.

The bandgap was then estimated from the linear extrapolation of the plot to meet $(h\nu)$ axis.^[37] For **SnS1** and **SnS2**, the direct bandgap observed were 1.52 and 1.40 eV respectively, which were higher than the direct bandgap of SnS bulk (1.3 eV). Different studies have shown dissimilar direct bandgaps for SnS nanoparticles and films ranging from 1.3–1.92 eV. The blue shifts of about 0.22 and 0.10 eV indicated quantum-size effect in the SnS nanoparticles.^[34]

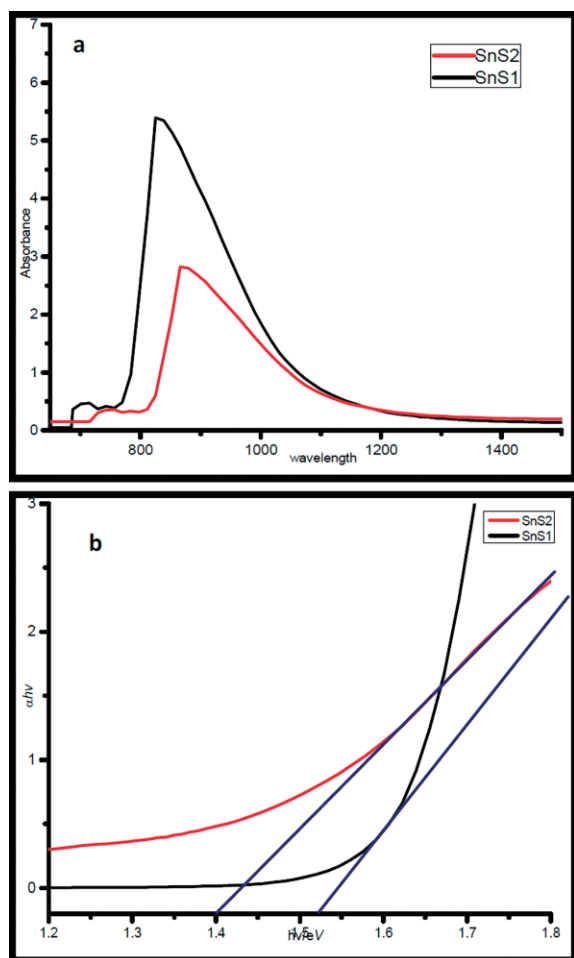


Figure 5. (a) UV/vis/NIR spectra and (b) TAUC plot of SnS2 and SnS1 nanoparticles.

Conclusions

The single source precursor, dibutyltin(IV) *p*-methylphenyl-dithiocarbamate complex, was successfully synthesized and used for the solvothermal synthesis of oleylamine (OLA) capped SnS nanoparticles. The two methods of solvothermal synthesis used in this work (heat up and hot-injection) resulted in different optical properties and sizes of the nanoparticles. The decomposition of the precursor complex in nitrogen atmosphere and in the absence of a capping agent resulted in a mixed oxidation-state phase of Sn₂S₃. The structural property revealed a herzenbergite structure of SnS with a pseudo spherical morphology which tends toward the formation of short rod in both methods of synthesis used. An average size of about 65 nm was estimated from the TEM analysis, while the optical property indicated quantum effect. The results from the analysis of the samples obtained from both approaches showed that the hot injection method gave more suitable SnS useful as a semiconductor.

Experimental Section

Materials and Methods: The chemicals were purchased from Sigma–Aldrich chemical Co, and used as received without further purification.

The ¹H, ¹³C and ¹¹⁹Sn NMR spectra (in DMSO) were either obtained with a Bruker Avance III 600 MHz or a Bruker Ascend 500 MHz Avance III HD (equipped with BBO) with the later using (CH₃)₄Sn as an external standard. Elemental analyses of C, H, N, and S in percentages were obtained with a Elementar, Vario EL Cube, whereas the infrared spectra, were recorded with a Bruker alpha-P FT-IR spectrophotometer. Thermogravimetric analysis (TGA/DTG) was carried out with a SDTQ 600 Thermal analyser, with data recording from 50–700 °C at a heating rate of 10 °C/min. The crystalline phases of the nanoparticles were identified by X-ray diffraction (XRD) measurements, with a scanning rate of 0.0018°·min⁻¹, using a Röntgen PW3040/60 X'Pert Pro XRD diffractometer equipped with nickel filtered Cu-K_α radiation (λ = 1.5418 Å) at room temperature. The optical properties of the nanoparticles were studied using a Jobin Yvon Lab-RAM HR 800 UV/Vis/NIR spectrophotometer using toluene as solvent. The morphology of the nanoparticles was characterized using a TECNAI G2 (ACI) TEM with an accelerating voltage of 200 kV.

Synthesis of Sodium *p*-Methyl-phenyldithiocarbamate (NaL): The preparation of the ligand (NaL) was achieved by slightly modifying a previously reported procedure.^[29] *p*-Methylaniline (0.01 mol) was dissolved in 10 mL tetrahydrofuran and reacted with a 20 mL tetrahydrofuran solution of NaOH (0.01 mol) in a nitrogen atmosphere. Carbon disulfide (0.01 mol) was added dropwise via a syringe into the solution. This mixture was stirred for 4–5 h at room temperature and filtered. The residue obtained was washed with diethyl ether to afford pale yellow solids, which were dried under vacuum.

Synthesis of the Dibutyltin(IV) *p*-Ethylphenyldithiocarbamate Complex [(C₄H₉)₂SnL₂]: Dibutyltin(IV) chloride (0.005 mol) was dissolved in 10 mL cold ethanol and added dropwise to the freshly prepared ethanolic solution of NaL. The solution was stirred for about 2 h in an ice bath. White precipitates were formed, filtered, washed with excess ethanol and dried under vacuum for 24 h. Recrystallization to obtain pure samples was achieved in a mixture of dichloromethane and ethanol. Yield: 2.63 g (73.66%); M.p.: 190–191 °C. **FT-IR** (selected bands) $\tilde{\nu}$ = 1516 (C=N), 1261 (C₂-N), 1004 (C=S), 2957 (–CH), 3085 (=CH), 3148 (N–H) 546 (Sn–C), 366 (Sn–S) cm⁻¹. **¹H NMR** (DMSO): δ = 7.47–7.12 (m, 8 H, N-C₆H₄), 2.50 (s, 6 H, Ar-CH₃), 5.29 (s, 2 H, N-H), 2.31 (t, 4 H, Sn-CH₂CH₂CH₂CH₃), 1.81 (m, 4 H, Sn-CH₂CH₂CH₂CH₃), 1.36 (m, 4 H, Sn-CH₂CH₂CH₂CH₃), 0.90 (t, 6H Sn-CH₂CH₂CH₂CH₃) ppm. **¹³C NMR** (DMSO): δ = 192 (–NCS₂), 136.9, 133.2, 129.1, 123.5 (–C₆H₅), 20.4 (Ar-CH₃), 27.5 (Sn-CH₂CH₂CH₂CH₃), 26.1 (Sn-CH₂CH₂CH₂CH₃), 25.8 (Sn-CH₂CH₂CH₂CH₃), 13.4 (Sn-CH₂CH₂CH₂CH₃) ppm. **¹¹⁹Sn NMR** (CDCl₃): δ = –312.0 ppm. C₂₄H₃₄N₂S₄Sn (598.06): calcd. C, 48.24; H, 5.74; N, 4.69; S, 21.47%; found: C, 47.84; H, 6.04; N, 4.19; S, 22.00 %

Keywords: Organotin(IV) dithiocarbamate; Tin; Sulfide; Nanoparticles; Optical properties

References

- [1] G. Zhang, Z. Fu, Y. Wang, H. Wang, *Adv. Powder Technol.* **2015**, 26, 1183.
- [2] R. E. Abutbul, E. Segev, L. Zeiri, V. Ezersky, G. Makov, Y. Golan, *RSC Adv.* **2016**, 6, 5848.
- [3] K. Ramasamy, V. L. Kuznetsov, K. Gopal, M. A. Malik, J. Raftery, P. P. Edwards, P. O'Brien, *Chem. Mater.* **2013**, 25, 266.
- [4] S. G. Hickey, C. Waurisch, B. Rellinghaus, A. Eychmüller, *J. Am. Chem. Soc.* **2008**, 130, 14978.

- [5] A. T. Kana, T. G. Hibbert, M. F. Mahon, K. C. Molloy, I. P. Parkin, L. S. Price, *Polyhedron* **2001**, *20*, 2989.
- [6] N. Koteeswara Reddy, M. Devika, E. S. R. Gopal, *Crit. Rev. Solid State Mater. Sci.* **2015**, *40*, 359.
- [7] J. Zhu, H. Wang, *Encycl. Nanosci. Nanotechnol.* **2013**, 1.
- [8] S. Sohila, M. Rajalakshmi, C. Ghosh, A. K. Arora, C. Muthamizhchelvan, *J. Alloys Compd.* **2011**, *509*, 5843.
- [9] Y. Zhao, Z. Zhang, H. Dang, W. Liu, *Mater. Sci. Eng. B* **2004**, *113*, 175.
- [10] N. K. Youn, H. R. Jung, J. Gwak, A. Cho, S. J. Ahn, S. K. Ahn, J. H. Kim, Y.-J. Eo, D. H. Kim, *Thin Solid Films* **2018**, *660*, 294.
- [11] A. de Kergommeaux, M. Lopez-Haro, S. Pouget, J.-M. Zuo, C. Lebrun, F. Chandezon, D. Aldakov, P. Reiss, *J. Am. Chem. Soc.* **2015**, *137*, 9943.
- [12] A. Roffey, N. Hollingsworth, H.-U. Islam, M. Mercy, G. Sankar, C. R. A. Catlow, G. Hogarth, N. H. de Leeuw, *Nanoscale* **2016**, *8*, 11067.
- [13] S. Tiwari, K. Reddy, A. Bajpai, K. Khare, V. Nagaraju, *Int. Res. J. Pure Appl. Chem.* **2015**, *7*, 78.
- [14] N. Srinivasan, S. Thirumaran, S. Ciattini, *J. Mol. Struct.* **2014**, *1076*, 382.
- [15] D. C. Menezes, G. M. De Lima, A. O. Porto, C. L. Donnici, J. D. Ardisson, A. C. Doriguetto, J. Ellena, *Polyhedron* **2004**, *23*, 2103.
- [16] A. A. Memon, M. Afzaal, M. A. Malik, C. Q. Nguyen, P. O'Brien, J. Raftery, *Dalton Trans.* **2006**, 4499.
- [17] D. C. Onwudiwe, P. A. Ajibade, *Int. J. Mol. Sci.* **2011**, *12*, 5538.
- [18] X. Hu, G. Song, W. Li, Y. Peng, L. Jiang, Y. Xue, Q. Liu, Z. Chen, J. Hu, *Mater. Res. Bull.* **2013**, *48*, 2325.
- [19] G. Barone, T. Chaplin, T. G. Hibbert, A. T. Kana, M. F. Mahon, K. C. Molloy, I. D. Worsley, I. P. Parkin, L. S. Price, *J. Chem. Soc., Dalton Trans.* **2002**, 1085.
- [20] D. C. Menezes, G. M. De Lima, F. A. Carvalho, M. G. Coelho, A. O. Porto, R. Augusti, J. D. Ardisson, *Appl. Organomet. Chem.* **2010**, *24*, 650.
- [21] J. O. Adeyemi, D. C. Onwudiwe, M. Singh, *J. Mol. Struct.* **2019**, *1179*, 366.
- [22] M. Sarwar, S. Ahmad, S. Ahmad, S. Ali, S. A. Awan, *Trans. Met. Chem.* **2007**, *32*, 199.
- [23] J. O. Adeyemi, D. C. Onwudiwe, A. C. Ekennia, R. C. Uwaoma, E. C. Hosten, *Inorg. Chim. Acta* **2018**, *477*, 148.
- [24] M. Sirajuddin, S. Ali, M. N. Tahir, *Inorg. Chim. Acta* **2016**, *439*, 145.
- [25] N. K. Kaushik, B. Bhushan, A. K. Sharma, *Trans. Met. Chem.* **1985**, *255*, 250.
- [26] D. C. Onwudiwe, T. Arfin, C. A. Strydom, R. J. Kriek, *Electrochim. Acta* **2013**, *109*, 809.
- [27] M. A. Affan, M. A. Salam, F. B. Ahmad, F. White, H. M. Ali, *Inorg. Chim. Acta* **2012**, *387*, 219.
- [28] N. Awang, I. Baba, B. M. Yamin, MS Othman, N. F. Kamaludin, *Am. J. Appl. Sci.* **2011**, *8*, 310.
- [29] D. C. Onwudiwe, T. Arfin, C. A. Strydom, R. J. Kriek, *Electrochim. Acta* **2013**, *109*, 419.
- [30] S. H. Chaki, M. D. Chaudhary, M. P. Deshpande, *Adv. Nat. Sci. Nanosci. Nanotechnol.* **2014**, *5*, 045010.
- [31] V. S. R. R. Pullabhotla, M. W. Mabila, *Mater. Lett.* **2016**, *183*, 30.
- [32] J. Henry, K. Mohanraj, S. Kannan, S. Barathan, G. Sivakumar, *J. Exp. Nanosci.* **2015**, *10*, 78.
- [33] S. Mourdikoudis, L. M. Liz-Marzán, *Chem. Mater.* **2013**, *25*, 1465.
- [34] J. Ning, K. Men, G. Xiao, L. Wang, Q. Dai, B. Zou, B. Liu, G. Zou, *Nanoscale* **2010**, *2*, 1699.
- [35] D. C. Onwudiwe, C. Strydom, O. S. Oluwafemi, S. P. Songca, *Mater. Res. Bull.* **2012**, *47*, 4445.
- [36] N. G. Deshpande, A. A. Sagade, Y. G. Gudage, C. D. Lokhande, R. Sharma, *J. Alloys Compd.* **2007**, *436*, 421.
- [37] M. Pal, A. Martinez Ayala, N. R. Mathews, X. Mathew, *J. Nano Res.* **2014**, *28*, 91.

Received: March 21, 2019

Published Online: ■

*J. O. Adeyemi, O. A. Oyewo, D. C. Onwudiwe** 1–7
Optical and Structural Properties of Tin Sulfide Nanoparticles
Obtained via Solvothermal Routes

